

# Discovery of very extended emission-line region around the Seyfert 2 galaxy NGC 4388 <sup>1</sup>

Michitoshi Yoshida<sup>2,3</sup>, Masafumi Yagi<sup>2</sup>, Sadanori Okamura<sup>4,5</sup>, Kentaro Aoki<sup>6,7</sup>, Youichi Ohyama<sup>8</sup>, Yutaka Komiyama<sup>8</sup>, Naoki Yasuda<sup>6</sup>, Masanori Iye<sup>2</sup>, Nobunari Kashikawa<sup>2</sup>, Mamoru Doi<sup>7</sup>, Hisanori Furusawa<sup>4</sup>, Masaru Hamabe<sup>11</sup>, Masahiko Kimura<sup>10</sup>, Masayuki Miyazaki<sup>4</sup>, Satoshi Miyazaki<sup>9</sup>, Fumiaki Nakata<sup>4</sup>, Masami Ouchi<sup>4</sup>, Maki Sekiguchi<sup>10</sup>, Kazuhiro Shimasaku<sup>4</sup>, AND Hiroshi Ohtani<sup>12</sup>

## ABSTRACT

We found a very large,  $\sim 35$  kpc, emission-line region around the Seyfert type 2 galaxy NGC 4388, using deep narrow-band imaging with the prime focus camera (Suprime-Cam) of the Subaru telescope. This region consists of many faint gas clouds or filaments, and extends northeastwards from the galaxy. The typical H $\alpha$  luminosity  $L(\text{H}\alpha)$  of the clouds is  $\sim 10^{37}$  erg s<sup>-1</sup>, and the total  $L(\text{H}\alpha)$  of the region within 10 kpc from the nucleus is  $\sim 2 \times 10^{38}$  erg s<sup>-1</sup>, which corresponds to an ionized gas mass of  $\sim 10^5 M_{\odot}$ . The map of the emission-line intensity ratio  $I([\text{O III}])/I(\text{H}\alpha)$  indicates that the inner ( $r < 12$  kpc) region of the VEELR may be excited by nuclear ionizing radiation. The excitation mechanism of the outer ( $r > 12$  kpc) region is unclear, but it is likely that the nuclear radiation is also a dominant source of its ionization. We discuss the origin of the ionized gas. Two plausible origins of the gas in the VEELR are (i) the tidal debris resulting from a past interaction with a gas-rich dwarf galaxy, i.e., a minor merger, or (ii) the interstellar medium of NGC 4388, stripped by the ram pressure of the hot intracluster medium of the Virgo cluster.

*Subject headings:* galaxies: individual (NGC 4388) — galaxies: Seyfert — galaxies: halos — galaxies: interactions — intergalactic medium

---

<sup>2</sup>Optical and Infrared Astronomy Division, National Astronomical Observatory, Mitaka, Tokyo, 181-8588 Japan.

<sup>3</sup>Okayama Astrophysical Observatory, National Astronomical Observatory, Kamogata, Okayama, 719-0232 Japan; yoshida@oao.nao.ac.jp.

<sup>4</sup>Department of Astronomy, School of Science, University of Tokyo, Tokyo, 113-0033 Japan.

<sup>5</sup>Research Center for the Early Universe, School of Science, University of Tokyo, Tokyo, 113-0033 Japan.

<sup>6</sup>Astronomical Data Analysis Center, National Astronomical Observatory, Mitaka, Tokyo, 181-8588 Japan.

<sup>7</sup>Institute of Astronomy, School of Science, University of Tokyo, Mitaka, Tokyo, 181-8588 Japan.

<sup>8</sup>Subaru Telescope, National Astronomical Observatory of Japan, 650 North A'Ohoku Place, Hilo, HI 96720 USA.

<sup>9</sup>Advanced Technology Center, National Astronomical Observatory, Mitaka, Tokyo, 181-8588 Japan.

<sup>10</sup>Institute for Cosmic Ray Research, University of Tokyo, Kashiwa, Chiba, 277-8582 Japan.

<sup>11</sup>Department of Mathematical and Physical Sciences,

## 1. INTRODUCTION

It is widely recognized that extended emission-line regions are commonly associated with active galactic nuclei (AGNs), and that most of them are photoionized by the nuclear power-law ionizing continuum. The extended emission-line regions of AGNs are often in the shape of a cone, whose apex corresponds to the nucleus. This trend is generally interpreted as evidence for anisotropy of the nuclear radiation of AGNs (e.g., Pogge 1989;

---

Faculty of Science, Japan Women's University, Bunkyo-ku, Tokyo, 112-8681 Japan.

<sup>12</sup>Department of Astronomy, Faculty of Science, Kyoto University, Sakyo-ku, Kyoto, 606-8502 Japan.

<sup>1</sup>Based on data collected at Subaru Telescope, which is operated by the National Astronomical Observatory of Japan.

Mulchaey, Wilson, & Tsvetanov 1996; Falcke, Wilson & Simpson 1998).

NGC 4388 is one of the nearest Seyfert 2 galaxies, and the first Seyfert to be found in the Virgo cluster (Phillips & Malin 1982). NGC 4388 is located within  $1^\circ$  of the two cD galaxies, M84 and M86, which lie at the center of the Virgo cluster (Binggeli, Tamman & Sandage 1987). Although the recession velocity of NGC 4388 ( $2540 \text{ km s}^{-1}$ ) is substantially larger than the cluster mean velocity of  $1100 \text{ km s}^{-1}$ , its distance estimated from the Tully-Fisher relation (16.7 Mpc) is close to that of the cluster center (Yasuda, Okamura & Fukugita 1997). The spatial location of the galaxy is thus very close to the core of the cluster. At a distance of 16.7 Mpc,  $1'$  corresponds to 4.86 kpc.

NGC 4388 is associated with a large, bright optical emission-line region (Pogge 1988; Corbin, Baldwin & Wilson 1988; Ayani & Iye 1989; Veilleux et al. 1999a, hereafter VBCTM, and references therein). The extended emission-line region (EELR) of NGC 4388 is characterized by at least three components: 1) a low-ionization disk component, 2) a high-ionization cone-shaped component extending southwestwards from the nucleus (hereafter referred to as the “SW cone”), and 3) a large high-ionization plume extending northeastwards from the nucleus up to 4 kpc above the plane of the galaxy (hereafter referred to as the “NE plume”) (Pogge 1988; Corbin et al. 1988; Colina 1992; Falcke et al. 1998; VBCTM). The low-ionization component is attributed to a complex of disk H II regions. The excitation properties of the gas in the SW cone and the NE plume resemble those of the nuclear narrow-line region gas, and are consistent with power-law photoionization models, indicating that anisotropic ionizing radiation from the Seyfert nucleus forms these regions (Pogge 1988; Petitjean and Durret 1993). The NE plume extends further than the SW cone, which is in front of the galaxy disk and consequently suffers less from dust obscuration. The shape of the NE plume is remarkable; it extends along P.A.  $\approx 30^\circ$  from the nucleus like a wide belt, and curls towards the northwest at a distance of  $\approx 3$  kpc (VBCTM). The total length of the NE plume is up to 4 kpc. The origin of the NE plume is still controversial, although several models have been proposed: tidal debris from a galaxy-galaxy encounter (Pogge 1988), gas stripped from the

galaxy disk by ram pressure induced by interaction with the intracluster gas (Petitjean & Durret 1993), ejecta from supernovae in the disk (Corbin et al. 1988), or a nuclear outflow powered by the radio jet (VBCTM).

In this paper, we report the discovery of a very extended emission-line region around NGC 4388, in deep, narrow-band images made with the Subaru telescope. The extension of the emission-line region is more than eight times greater than that of the previously found emission, extending as far as 35 kpc from the nucleus. We describe the observations and data reduction in §2, and present the results in §3. In §4 we briefly discuss possible models for the origin of the emission-line gas and comment on its relationship to the inner emission-line region. We summarize our study in §5.

## 2. OBSERVATIONS AND DATA REDUCTION

The narrow-band and broad-band imaging observations were made with the Suprime-Cam (Miyazaki et al. 1998; Iye et al. 1997) attached at the prime focus of the Subaru telescope (Kaifu et al. 2000) on 2001 March 24 and 2001 April 24 and 26. In the March run, the camera consisted of 9 CCDs; four SITe  $2K \times 4K$  CCDs and five MIT  $2K \times 4K$  CCDs. After the March run, all the SITe CCDs were replaced by new MIT CCDs, so 10 MIT CCDs were used in the April run. The pixel size was  $15 \mu\text{m}$ , which corresponds to 0.2 arcsec on the sky. The H $\alpha$ + [N II] narrow-band imaging of NGC 4388 was performed on 2001 April 26 with a narrow-band filter whose central wavelength,  $\lambda_0$ , and FWHM were 6600 Å and 100 Å, respectively (filter N-A-L659). The [O III]  $\lambda 5007$  Å imaging was carried out on 2001 April 24, using a filter whose  $\lambda_0$  and FWHM were 5020 Å and 100 Å respectively (filter N-A-L503). To subtract the continuum component from the narrow-band images so as to extract a pure emission-line image, we obtained  $R_c$ -band and  $V$ -band images, which allowed us to estimate the continuum in the H $\alpha$ + [N II] image and [O III] image, respectively. The broad-band data were taken on 2001 March 24. The observations are summarized in Table 1. The seeing was  $0''.6 - 0''.7$  on the nights of the narrow-band imaging observations, and  $0''.9 - 1''.0$  on the nights of the broad-band imaging.

The sky was clear, but not photometric, on these nights; however, some photometric standard stars were obtained for rough flux calibration.

Data reduction was performed using IRAF and DASH (Mizumoto et al. 2000; Yagi et al. 2000), which is a pipeline data reduction system in a distributed computing environment. Basic data reduction procedures, i.e., bias and dark subtraction, flat fielding, and distortion correction, were carried out using a data reduction pipeline developed specifically for Suprime-Cam data under the DASH environment. Since significant non-uniformity ( $\approx 5\%$  at peak-to-peak) was found in the flat field frames of the filter N-A-L659, the flat-fielded  $H\alpha$ + $[N\ II]$  images have a large-scale non-uniform pattern over a CCD frame. The cause of this non-uniformity has not yet been identified. We fitted the pattern with a cubic polynomial and subtracted the fitted function from the object frames after the ordinary flat-fielding procedure. Therefore, the internal accuracy of photometry in N-A-L659 frames should be at worst  $\sim \pm 5\%$ , which is accurate enough for this study.

The CCD was saturated at and around the nucleus of the galaxy in all the object frames taken. In the narrow-band frames, the region of radius  $r < 3$  arcsec centered on the nucleus was affected by saturation. In the broad-band frames, the saturation was more severe and the whole central region ( $r < 15$  arcsec) could not be used for data analysis (see Figs 1c and 1d). Part of the inner spiral arms was also saturated in the  $R_c$ -band frames (Fig. 1c).

The flat-fielded frames in the same bands were aligned using field stars and co-added to improve the signal-to-noise ratio. For each of the co-added frames a quadratic curved surface was fitted to the sky background well outside the galaxy disk and subtracted from the image. In order to make an uncontaminated  $H\alpha$ + $[N\ II]$  image, the  $R_c$ -band frame was scaled so that the average counts in the featureless part of the galaxy disk equaled those in the  $H\alpha$  frame; this scaled  $R_c$ -band frame was then subtracted from the  $H\alpha$ + $[N\ II]$  frame. When subtracting, PSF equalization was performed, following the method of Alard and Lupton (1998). The same procedure was applied to the  $[O\ III]$  frame and the  $V$ -band frame to extract a pure  $[O\ III]$  emission-line image.

Flux calibrations were carried out using our ob-

servations of spectrophotometric standard stars. As mentioned above, the observing conditions were not photometric; fluxes of standard stars obtained at similar elevations varied by up to  $\sim 10\%$ . Moreover, differences in the effective transmission wavelengths between the narrow and broad observing bands reduce the photometric accuracy in regions, such as the shoulder of the bulge, where large color gradients may exist. For the  $H\alpha$ + $[N\ II]$  ( $\lambda_0 = 6590\ \text{\AA}$ ) and the  $R_c$  ( $\lambda_0 \sim 6700\ \text{\AA}$ ) bands, the central wavelength difference is small enough that the color difference may be ignored. On the other hand, the color difference between the  $[O\ III]$  filter ( $\lambda_0 = 5020\ \text{\AA}$ ) and the  $V$ -band filter ( $\lambda_0 \sim 5500\ \text{\AA}$ ) is not negligible. The flux difference between  $\lambda 5000\ \text{\AA}$  and  $\lambda 5500\ \text{\AA}$  for Sb galaxies is  $\sim 5\%$ , according to Coleman, Wu and Weedman (1980).

We also examined the amount of emission-line flux that might have fallen outside the filter band pass due to the redshift of the object. We found that the loss of flux is 20% at most, even if the recession velocity of emission-line clouds is  $300\ \text{km s}^{-1}$  over the systemic velocity of NGC 4388. Combining this uncertainty with the flux calibration error due to the non-photometric conditions, we estimate that the uncertainty in the flux of our narrow-band images is typically 20%, but could be up to 50% at worst. Comparing our data with the spectrophotometric observations of Petitjean and Durret (1993), we found our flux at  $35''$  away from the nucleus at P.A. =  $55^\circ$  to be consistent with theirs to within 30%.

### 3. RESULTS

The continuum-subtracted  $H\alpha$ + $[N\ II]$  and  $[O\ III]\lambda 5007\ \text{\AA}$  images and the broad-band images of NGC 4388 are shown in Figs. 1a – 1d. The  $H\alpha$ + $[N\ II]$  image is the deepest emission-line image of NGC 4388 ever taken. The detection limits are as faint as  $\sim 2 \times 10^{-19}\ \text{erg s}^{-1}\ \text{cm}^{-2}\ \text{arcsec}^{-2}$  for the  $H\alpha$ + $[N\ II]$  image (Fig. 1a), and  $\sim 3 \times 10^{-18}\ \text{erg s}^{-1}\ \text{cm}^{-2}\ \text{arcsec}^{-2}$  for the  $[O\ III]$  image (Fig. 1b).

A remarkable feature of these images is the large number of extended emission-line filaments that are clearly seen in both the  $H\alpha$ + $[N\ II]$  and  $[O\ III]$  images. (Hereafter, we call the region of these filaments the very extended emission-line

region, or VEELR.) The VEELR extends very far outside the galaxy disk ( $r > 1'$ ) between P.A.  $\sim 30^\circ$  and P.A.  $\sim 65^\circ$ . A sketch of the VEELR is shown in Fig. 2. The most distant cloud/filament seen in the  $H\alpha$  image is at  $\approx 430''$  ( $\approx 35$  kpc) northeast of the nucleus. This distant cloud/filament is marginally seen also in the [O III] image (Fig. 1b). A close-up view of the VEELR is shown in Fig. 3, where major clouds/filaments are identified by numbers. There seem to be two streams in the VEELR; one starts at  $90''$  from the nucleus along P.A.  $\approx 55^\circ$  and curves smoothly to the north at P.A.  $\approx 10^\circ$ , with a total length of up to  $120''$ , and the other extends between P.A.  $\approx 50^\circ$  and P.A.  $\approx 65^\circ$  from  $120''$  from the nucleus out to more than  $300''$ . The latter stream is further divided into two streams at  $200''$  from the nucleus, one of which is a smooth emission region extended along P.A.  $\approx 60^\circ$  (OF-1 in Fig. 3) and the other is a faint string of clouds extended along P.A.  $\approx 0^\circ - -20^\circ$  (C22, C23, C24). At  $300''$  from the nucleus, there is a large complex of clouds (OF-2), and the stream bends to the north, extending up to  $430''$  away. The most distant clouds/filament complex (OF-5) is curved like a bow whose string is directed toward the nucleus. The luminosity in  $H\alpha + [\text{N II}]$  of a typical cloud/filament in the VEELR is  $\sim 10^{37}$  erg  $\text{s}^{-1}$ .

The ionized gas mass of each cloud/filament is calculated using the relation

$$M_{\text{gas}} = V N_e(\text{rms}) f_v^{1/2} m_H,$$

where  $V$  is the volume of the filament,  $N_e(\text{rms})$  is the rms value of electron density,  $f_v$  is volume filling factor, and  $m_H$  is the mass of a hydrogen atom.  $N_e(\text{rms})$  is derived from the following equation (Yoshida & Ohtani 1993):

$$N_e(\text{rms}) (\text{cm}^{-3}) = 1.2 \times \left( \frac{V}{10^6 \text{pc}^3} \right)^{-1/2} \left( \frac{L(H\alpha)}{10^{37} \text{erg s}^{-1}} \right)^{1/2}$$

We assumed Case B recombination and the electron temperature  $T_e = 10^4$  K in this calculation. Although the volume filling factor  $f_v$  is not known for the VEELR clouds, a typical value for such extranuclear emission-line gas is  $\sim 10^{-3} - 10^{-4}$  (Yoshida & Ohtani 1993; Robinson et al. 1994; Aoki et al. 1994). Since the typical  $H\alpha$  luminosity and size of a cloud/filament in the VEELR are  $\sim 10^{37}$  erg  $\text{s}^{-1}$  and a few hundred pc, respectively,

its rms electron density is  $\sim 0.3 - 0.4 \text{ cm}^{-3}$ , assuming a spherical geometry for the cloud. Therefore, if the local electron density of emission-line clouds is  $N_e(\text{local}) \sim 10$ , we infer  $f_v \sim 2 \times 10^{-3}$ , because  $N_e(\text{local})$  is related to  $N_e(\text{rms})$  and  $f_v$  by the equation  $N_e(\text{rms}) = f_v^{1/2} N_e(\text{local})$ . If this is the case, the mass of a typical cloud is  $\sim 10^3 M_\odot$ .

The sizes, distances from the nucleus, ionized gas masses, and emission-line fluxes of the gas clouds/filaments in the VEELR of NGC 4388 are listed in Table 2. The volume of each cloud/filament was calculated assuming an ellipsoid whose major axis is the projected major axis of each cloud/filament for compact, bright ones (C1 - C26). We assumed a sheet-like morphology for the diffuse filaments (e.g filaments in OF-1 - OF-5) whose thickness along our line of sight is 100 pc. The total mass of the ionized gas of the VEELR is  $\sim 4 \times 10^6 f_v^{1/2} M_\odot$ . This is comparable to that of the NE plume derived by VBCTM,  $\sim 10^5 M_\odot$ , if  $f_v \sim 1 \times 10^{-3}$ .

The morphology of the bright part of the emission-line region in our images (the disk H II region, the NE plume, and the SW cone) is similar to that found in previous studies (Pogge 1988; Corbin et al. 1988, VBCTM), but more detailed structure is revealed. Fig. 4 shows a close-up of the NE plume. (In order for the spatial structure of the emission-line region to be clearly seen, PSF equalization, which degrades the spatial resolution of the image, was not performed in making this figure.) The NE plume consists of many filaments whose widths are marginally resolved at our resolution ( $\approx 0''.8$ ) and are about 80 - 100 pc ( $\approx 1''$ ).

A map of the emission-line intensity ratio  $I([\text{O III}])/I(H\alpha + [\text{N II}])$  is shown in Fig. 5. This map is very useful for investigating the excitation structure of the outer emission-line region, although the detailed structure of the gas excitation distribution near the nucleus is totally lost in this figure, because of severe saturation of the broad-band images. Nevertheless, a distinct cone-like structure of high excitation gas is clearly seen to the south of the nucleus. This ‘‘ionization cone’’ was first found by Pogge (1988) and its structure has been investigated in several studies (Pogge 1988; Falcke et al. 1998, VBCTM). The north side of the ionization cone is traced by the NE plume

and a high-ionization cloud located at  $10'' - 15''$  northwest of the nucleus. We note that filaments of the inner VEELR ( $\lesssim 10$  kpc; C1 – C8) also show high ionization,  $I([\text{O III}])/I(\text{H}\alpha) \gtrsim 1$ , suggesting that these filaments are also excited by the nuclear ionizing radiation. Interestingly, the filaments at about 11 kpc from the nucleus show an internal excitation gradient; the  $I([\text{O III}])/I(\text{H}\alpha)$  ratio smoothly decreases with distance from the nucleus in one filament (C2, C3, C4) (Fig. 5). In addition, we note that a bright filament at P.A. =  $70^\circ$ , 11 kpc away from the nucleus (C25) shows quite low excitation ( $I([\text{O III}])/I(\text{H}\alpha) \sim 0.1$ ), although its projected distance from the nucleus is the same as those of clouds C9 – C15. There seems to be a sudden change in the excitation state of the gas at around the line of P.A. =  $65^\circ$ , which coincides with the extrapolation of the northern edge line of the SW cone. These findings suggest that the nuclear ionization cone excites most of the VEELR gas. The excitation mechanism of the VEELR will be discussed further in the next section.

## 4. DISCUSSION

### 4.1. The excitation mechanism of the very extended emission-line region of NGC 4388

Figure 6 shows the radial variation of the emission-line intensity ratio,  $I([\text{O III}])/I(\text{H}\beta)$ . In this figure the  $\text{H}\beta$  flux in the VEELR is derived from the  $\text{H}\alpha + [\text{N II}]$  flux by assuming that (1) the gas is in Case B recombination with an electron temperature of  $10^4$  K ( $I(\text{H}\alpha)/I(\text{H}\beta) = 2.86$ ; Osterbrock 1989), (2) the  $I([\text{N II}])/I(\text{H}\alpha)$  emission-line intensity ratio is 0.2, and (3) there is no dust extinction. Since most of the VEELR is located well outside the galactic disk of NGC 4388, the above assumptions are adequate to estimate the  $\text{H}\beta$  flux. The  $I([\text{O III}])/I(\text{H}\beta)$  ratio decreases with distance from the nucleus.

Although it is impossible to estimate the excitation mechanism of the ionized gas uniquely using only the  $I([\text{O III}])/I(\text{H}\beta)$  intensity ratio, the monotonic decrease of this ratio with radius suggests that the same mechanism is responsible for exciting the gas in these regions. The NE plume has a similar emission-line spectrum to that of the nucleus; the spectrum is consistent with power-law photoionization models with an ionization pa-

rameter  $U \sim 10^{-3}$  (Pogge 1988; Petitjean & Durret 1993). Since the distance from the nucleus of the VEELR is 3 – 4 times that of the NE plume, the number of ionizing photons from the nucleus that reach the VEELR is smaller by  $1/9 - 1/16$  times. Thus, assuming that the gas density decreases with  $r^{-1}$ , one finds that  $U$  for the VEELR is a few times  $10^{-4}$ . Power-law photoionization models predict that  $I([\text{O III}])/I(\text{H}\beta) \approx 1 - 3$  for such values of  $U$ . This is consistent with the observed values of the emission-line intensity ratio.

In the case of nuclear power-law photoionization, the number of nuclear ionizing photons necessary to ionize the VEELR is estimated by the following relation:

$$Q_{\text{u}} = 4\pi R^2 c N_{\text{e}} U,$$

where  $R$  is the distance of an VEELR cloud from the nucleus,  $c$  is the speed of light,  $N_{\text{e}}$  and  $U$  are the electron density and the ionization parameter of the cloud, respectively. Assuming that  $N_{\text{e}} \sim 10 \text{ cm}^{-3}$  and  $U \sim 10^{-4}$ , one finds that  $Q_{\text{u}}$  is a several times  $10^{53}$  photons  $\text{s}^{-1}$  for a cloud at a distance of  $\sim 10$  kpc from the nucleus. The value of  $Q_{\text{u}}$  derived above is a typical one of nearby type 1 Seyfert galaxies (e.g. Padovani and Rafanelli 1988; Yoshida and Ohtani 1993; Aoki et al. 1996). Taking into account the anisotropic nature of the nuclear radiation, we conclude that the nuclear power-law continuum of NGC 4388 is capable of ionizing most of the VEELR gas.

The observed values of  $I([\text{O III}])/I(\text{H}\beta)$  in the VEELR are, on the other hand, also consistent with expectations for other excitation mechanisms, such as OB star ionization (H II regions) or shock heating. They agree with the predictions of models of H II regions with moderate metal abundances ( $[\text{O}/\text{H}] \sim [\text{O}/\text{H}]_{\odot}$ ) (McCall, Rybski & Shields 1985). However, there is no signature of ionizing star clusters near the VEELR. If the VEELR is ionized by UV radiation emanating from the disk star-forming complex, a total of  $\sim 2 \times 10^2$  O5 stars are needed to excite a typical  $\text{H}\alpha$  cloud in the VEELR ( $L(\text{H}\alpha) \sim 10^{37} \text{ erg s}^{-1}$ , the mean distance from the disk  $\approx 10$  kpc, and typical size of a cloud is 300 pc). On the other hand, the total number of ionizing stars estimated from the  $\text{H}\alpha$  luminosity of the disk H II complex is  $\sim 3 \times 10^2$ . These two numbers are consistent with each other. However, the actual number of disk-

ionizing stars needed to ionize the VEELR would be much larger than this estimate, because a significant part of the ionizing radiation is exhausted in ionizing the surrounding dense gas from which the stars were born. It is unlikely that such a large star-forming complex resides in the disk of NGC 4388.

Shock heating is another candidate excitation mechanism for the VEELR. Shocks whose velocities are  $\sim 100 \text{ km s}^{-1}$  can explain the observed  $I([\text{O III}])/I(\text{H}\beta)$  ratios of the VEELR (Schull & McKee 1979; Binette, Dopita & Tuohy 1985; Dopita & Sutherland 1995). The kinematics and emission-line intensity ratios of other species, such as  $I([\text{N II}])/I(\text{H}\alpha)$  or  $I([\text{S II}])/I(\text{H}\alpha)$ , of the VEELR gas are needed to estimate the contribution from shock heating. Nevertheless, we consider that shock heating is not the main source of the excitation of the VEELR, because the shock heating model cannot explain (1) the smooth radial decrease of the  $I([\text{O III}])/I(\text{H}\beta)$  ratio or (2) the sudden change of the  $I([\text{O III}])/I(\text{H}\alpha)$  ratio between the inside and outside of the ionization cone.

Therefore, it is likely that most of the VEELR is ionized and excited primarily by the nuclear ionizing radiation, although detailed spectroscopic study is needed to determine the excitation source precisely. (Note that the excitation mechanism of the low-ionization filaments outside the ionization cone (C25 and C26) is not identified. The  $[\text{O III}]$  emission is significantly fainter than the  $\text{H}\alpha$  in those filaments, and is not detectable in our images.)

#### 4.2. Origin of the very extended emission-line region of NGC 4388

The VEELR is very large ( $> 30 \text{ kpc}$ ) and extends only on the northeastern side of the galaxy. Here, we discuss the origin of the VEELR of NGC 4388.

##### 4.2.1. AGN wind

Gas outflow phenomena have often been detected around active galactic nuclei (e.g., Mediavilla & Arribas 1995; Aoki et al. 1996; Arribas, Mediavilla & Garcia-Lorenzo 1996; Veilleux et al. 1998). VBCTM suggested that the most plausible origin of the inner extraplanar ionized nebula of

NGC 4388 is a bipolar outflow, which was originally accelerated by the radio ejecta from the nucleus.

Energetically, the radio jet could have accelerated the ionized gas in the VEELR. The total mass of the VEELR gas is of order  $10^5 M_{\odot}$ , and its radial velocities should be as fast as those of the NE plume gas, i.e.,  $100 - 200 \text{ km s}^{-1}$ . Thus, the kinetic energy of the ionized gas of the VEELR is  $\sim 10^{52} \text{ erg}$ . Although the turbulent energy of the VEELR is not known because of a lack of detailed velocity information, it is likely to increase the total kinetic energy of the VEELR by a factor of only two or three. VBCTM argued that the radio jet of NGC 4388 could accelerate material that had a similar level of kinetic energy.

There are some problems in this scheme for the origin of the VEELR of NGC 4388. First, there is a large discrepancy between the P.A. of the radio jet and that of the VEELR. The radio ejecta of NGC 4388 have P.A.  $\sim 5^{\circ}$  (Hummel & Saikia 1991; Irwin, Saikia & English 2000), whereas the VEELR is extended in P.A.  $\sim 40^{\circ} - 60^{\circ}$ . VBCTM suggested that a slight discrepancy between the P.A. of the NE plume and the radio jet can be explained by buoyancy of the jet as a result of a density gradient perpendicular to the galaxy disk. The P.A. discrepancy between the VEELR and the jet is, however, much larger, and buoyancy effects alone cannot explain it. Secondly, there is the size difference between the radio jet and the VEELR. The VEELR is very large, reaching out to  $35 \text{ kpc}$  from the nucleus, so that its age is of order  $10^8 \text{ yr}$ . On the other hand, the radio jet has a length of only  $1 \text{ kpc}$ . Therefore, the VEELR is more than an order of magnitude older than the radio jet, even if they have similar outflow velocities.

Large precession coupled with intermittent activity, or dense gas that blocks the radio jet, might solve these problems, but we consider attributing such peculiar behavior to the jet as highly speculative. We conclude that a nuclear outflow powered by the radio jet is not a plausible origin of the VEELR gas.

##### 4.2.2. Debris of ancient starburst superwind

Strong starburst activity in the nuclear regions of a galaxy causes a powerful outflow from the galaxy (Heckman, Armus & Miley 1990). Such

“superwinds”, induced by the collective effect of supernovae and the stellar winds of OB stars in a starburst region, are sometimes strong enough to blow the interstellar gas in galaxies into intergalactic space. For example, the superwind of the well-studied starburst galaxy M82 has a mechanical luminosity of  $\sim 2.5 \times 10^{42}$  erg s $^{-1}$  and a momentum flux of  $\sim 2 \times 10^{34}$  dynes (Lehnert, Heckman & Weaver 1999), and optical filaments associated with the wind extend well outside ( $> 3$  kpc from) the galaxy disk (Bland & Tully, 1988; Shopbell & Bland-Hawthorn 1998). Recently, an H $\alpha$ -emitting region, which may be associated with the superwind, was discovered about 12 kpc to the north of M82 (Devine & Bally 1999; Lehnert et al. 1999). The twin bubble of H $\alpha$ -emitting gas of Arp 220 has a size of 14 kpc (Armus, Heckman & Miley 1989; Ohya et al. 2001). The size of the VEELR of NGC 4388 is comparable to, but somewhat larger than, those of the superwinds associated with these powerful starburst galaxies.

In fact, strong star-forming activity is occurring in the disk of NGC 4388, which is traced by all existing H $\alpha$  images (Pogge 1988; VBCTM; this study). The total H $\alpha$  luminosity of the NGC 4388 disk is  $\approx 10^{40}$  erg s $^{-1}$ , corresponding to a star-formation rate of  $10M_{\odot}$  yr $^{-1}$ , which is comparable to that of the prototypical starburst galaxy M82. Thus, it would be natural to consider that NGC 4388 generates a huge outflow due to its strong star-forming activity.

The highly asymmetrical distribution of the VEELR gas is, however, problematic for this superwind scenario. A superwind that is powerful enough to blow the interstellar gas into intergalactic space should blow on both sides of the disk, because the energy injected by the starburst is so high that the hot gas produced by the starburst should expand well beyond the disk scale height (e.g., Chevalier & Clegg 1985; Tomisaka and Ikeuchi 1988; Strickland and Stevens 2000). However, the VEELR is distributed only in the northeast quadrant of NGC 4388. Even if we consider the fact that the gas in the region is excited by the asymmetric nuclear radiation, so that the shape of the line emitting gas traces the path of the radiation, it is difficult to explain the total lack of any extension in the southwestern direction using the superwind model.

#### 4.2.3. *Ram pressure stripped gas*

NGC 4388 is located close to the center of the Virgo cluster. It has been suggested that it is currently at the bottom of the cluster potential because of its extremely high peculiar velocity, which is over 1000 km s $^{-1}$  relative to the systemic velocity of the cluster (Yasuda et al. 1997). Together with the H I gas deficiency and the sudden truncation of the H I gas within the galaxy disk, this has led many authors to suggest that the interstellar gas of NGC 4388 is affected by strong ram pressure due to a high-speed interaction with the intracluster medium (ICM), and that the outer part of the interstellar gas is stripped from the galaxy by the ram pressure (Cayatte et al. 1994).

Petitjean and Durret (1993) suggested that the extraplanar gas extending to 50'' away from the nucleus of NGC 4388 (the NE plume) could be this ram-pressure-stripped gas. Here, we examine whether the ram-pressure-stripping model can be applied to the VEELR.

Ram-pressure-stripped gas is blown away from a galaxy preferentially in the opposite direction to the galaxy’s motion relative to the ICM (Abadi, Moor & Bower 1999). NGC 4388 is an edge-on galaxy, whose inclination angle is 78°; its north side is the near side (Pogge 1988; Ayani & Iye 1989; VBCTM). The VEELR is extended to the northeast of the galaxy. Hence, if the VEELR is the ram-pressure-stripped gas due to the interaction between the galaxy disk and the ICM, NGC 4388 must have quite a large transverse velocity southwestwards in order to blow the interstellar gas to such a high galactic latitude. Considering the large radial component of the velocity relative to the ICM ( $\sim 1400$  km s $^{-1}$ ), one finds that NGC 4388 must have a transverse velocity of  $\sim 1500$  km s $^{-1}$ . If this is the case, the total collision velocity of NGC 4388 to the ICM is  $\sim 2000$  km s $^{-1}$  and its collision angle is approximately 30–40°. Numerical simulations of ram-pressure stripping made by Abadi et al. (1999) suggest that when the collision velocity and the angle are 2000 km s $^{-1}$  and 45°, respectively, ram-pressure-stripped gas is extended up to 10 – 15 kpc from the galaxy disk after 10 $^8$  yr has passed since the collision between the galaxy and the ICM (see Figures 3 and 4 of Abadi et al. 1999). Furthermore, the truncation radius of H I gas and the surface density of the disk of NGC

4388 are consistent with their  $45^\circ$  collision model (Abadi et al. 1999). Therefore, the ram-pressure-stripping hypothesis for the origin of the VEELR gas is a promising one, if NGC 4388 indeed has such very large transverse velocity.

However, VBCTM have argued that the transverse velocity of NGC 4388 is rather small with respect to its radial velocity, so that the galaxy is falling into the cluster core almost along our line of sight. In other words, NGC 4388 is colliding with the ICM nearly edge-on. If this were the case, ram-pressure-stripped gas would be blown along the galaxy disk (Abadi et al. 1999), and the VEELR should be a projection of a flow along the disk plane. Since the projected distance of the far-end of the VEELR from the galaxy disk is 10 kpc, the real distance would be as much as  $\approx 10 \times \cos^{-1} i \sim 50$  kpc (due to the inclination of the disk  $i = 78^\circ$ ). The morphology of the VEELR strongly suggests that the gas extends perpendicular to the galactic disk, and that such a flat elongation is not likely. Moreover, such extremely elongated filaments in the plane of the galaxy disk could not be illuminated by the nuclear ionization cone indicated by the circumnuclear ionization structure. Consequently, if the transverse velocity of NGC 4388 is small, it is hard to believe that the VEELR gas is the interstellar gas stripped by ICM ram pressure.

Therefore, knowledge of the value of the transverse velocity of NGC 4388 is the key to determining whether the ram-pressure-stripping hypothesis is plausible. It is, however, impossible to measure the transverse velocity directly. Hence, we cannot conclude that ram-pressure stripping is responsible for the VEELR. To investigate this subject further, it would be useful to know the velocity field of the VEELR, which could be measured by deep spectroscopy.

We note that the outer edge of the VEELR may be strongly affected by interaction with the ICM. According to VBCTM, a large Mach cone with an opening angle of  $\approx 80^\circ$  is formed around NGC 4388 by the interaction with the Virgo cluster ICM. The apex of the cone is at the leading edge of the H I disk of the galaxy. If this is the case, the height of the contact discontinuity of the bow shock is  $= R_{\text{HI}} \times \tan 40^\circ \approx 8-9$  kpc above the galaxy plane. This is well inside the extension of the VEELR. Thus, the outer part of the VEELR

may be severely affected by the shock. The peculiar morphology of the VEELR, particularly its apparent bending, may be due to this interaction with the ICM.

#### 4.2.4. *Tidal debris from galaxy-galaxy interaction*

Pogge (1988) suggested that the NE plume of NGC 4388 might be tidal debris from a past galaxy-galaxy interaction, like the Magellanic stream. VBCTM rejected the tidal debris scenario, because they did not detect any distorted kinematic signatures in the disk velocity field, and because it does not explain the correlation between the [O III] surface brightness and the kinematics of the NE plume clouds (blue-shifted clouds tend to have high surface brightness). Considering the large size and stream-like morphology of the VEELR, however, we consider that a tidal debris model is a good candidate to explain the origin of the VEELR gas.

NGC 4388 lies near the core of the Virgo cluster (Yasuda et al. 1997), where galaxy-galaxy encounters may be comparatively frequent. Phillips and Malin (1982) discussed the morphological anomaly of the outskirts of the disk of NGC 4388. They commented on a faint envelope surrounding the western edge of the galaxy. We have also found that the disk of NGC 4388 is moderately asymmetrical at a low surface brightness level in our broad-band images, and that a faint hump exists near the southwest edge ( $\sim 300''$  away from the nucleus) of the galaxy (see Figs. 1c and 1d). This hump is seen in both the  $R_c$ - and  $V$ -band images, and is not found in the pure emission-line image, so that it should be mainly composed of stars. In addition, the bulge of NGC 4388 is boxy (Veilleux et al. 1999b). The features described above are clearly seen in Fig. 7, which shows the isophotes of NGC 4388 made from our  $R_c$ -band images (Fig. 1c). It has gradually come to be recognized that galaxies with boxy bulges have experienced minor merging in the past (Mihos et al. 1995; Walker, Mihos & Hernquist 1996).

The numerical simulations of minor merging carried out by Walker et al. (1996) indicate that a minor merging excites a strong bar mode ( $m = 2$ ) instability in 1 Gyr after the merging and thickens the disk of the primary galaxy significantly. The edge-on view of the disk and satellite particle 1

Gyr after merging in the simulations of Walker et al. (1996) strikingly resembles our R-band image of NGC 4388. The thick, asymmetric morphology of the disk with faint humps extending perpendicular to the disk plane at its edge, seen in their simulations, are also present in our image, indicating that NGC 4388 may be a minor merger remnant seen  $\sim 1$  Gyr after the beginning of the merger event. If this was the case, and the satellite was a gas-rich dwarf galaxy, a long tidal tail of gas from the satellite would be left along the path of the encounter. In fact, such large tidal tails of gas have been found around some mergers in H I observations (Arp 219, Smith 1994; NGC 7252, Hibbard et al. 1994; Arp 299, Hibbard and Yun 1999). The morphological similarity between the results of numerical simulations (Hernquist & Mihos 1995; Walker et al. 1996) and our R-band image of NGC 4388, together with the stream-like morphology of the VEELR, lead us to a conclusion that NGC 4388 is a minor merger remnant and that the VEELR consists of dense gas clouds in the tidal tails (tidal debris) illuminated by nuclear power-law radiation.

A minor merger also concentrates interstellar gas in the nucleus of the primary galaxy, and may drive nuclear activity. Taniguchi (1999) has argued that minor mergers are one of the most plausible candidate processes for driving Seyfert activity. He proposed that Seyfert 2 galaxies are activated by a minor merger with a highly inclined orbit. If this is the case for NGC 4388, a past minor merger may not only have formed the tidal tail in which the VEELR gas clumps are embedded, but may also have induced its nuclear activity.

## 5. Summary

We have found an very extended emission-line region (VEELR) that extends up to  $\sim 35$  kpc from the type 2 Seyfert 2 galaxy NGC 4388. This region consists of many faint gas clouds/filaments and extends northeastwards from the galaxy. The map of emission-line intensity ratio,  $I([\text{O III}])/I(\text{H}\alpha)$ , suggests that the clouds in the inner ( $r < 12$  kpc) region of the VEELR are excited by nuclear ionizing radiation. Although the excitation mechanism of the clouds in the outer ( $r > 12$  kpc) region is unclear, those clouds might also be excited primarily by the nuclear radiation, since they are within the

nuclear ionization cone. We discussed the origin of this ionized gas, and concluded that it is most plausible that the VEELR gas is tidal debris due to a past interaction with a gas-rich dwarf galaxy. If NGC 4388 has a large transverse velocity, of the order  $10^3 \text{ km s}^{-1}$  toward the south of the galaxy, it is also possible that the VEELR was formed by ram-pressure stripping of the disk gas due to a high-speed collision between the galaxy disk and the hot ICM.

In any case, since the VEELR lies at a very high latitude with respect to the disk plane, it is certain that the VEELR contains valuable information about the halo gas of NGC 4388. Deep spectroscopy of the VEELR will not only tell us the nature of the VEELR gas, giving us more reliable information on its kinematics, excitation mechanism, and metal abundance, but will also allow us to consider the origin of the halo gas of NGC 4388. In this context, we emphasize that very extended faint ionized gas that is illuminated by powerful radiation, such as AGN radiation, may provide us with a unique opportunity to investigate the physical state of halo gas around galaxies. Wide-field, deep, narrow-band imaging and deep spectroscopy of the halos of galaxies exhibiting AGN activity will be useful in such studies.

We are grateful to the staff of the Subaru telescope for their kind help with the observations. We thank Y. Taniguchi and T. Nagao for useful discussions. We also thank anonymous referee for her/his comments on the manuscript. In addition, M. Y. thanks the staff of Okayama Astrophysical Observatory for their encouragement during the course of this study. This work was done using the facilities at the Astronomical Data Analysis Center, National Astronomical Observatory of Japan. This research has made use of NASA's Astrophysics Data System Abstract Service.

## REFERENCES

- Abadi, M. G., Moore, B., & Bower, R. G. 1999, *MNRAS*, 308, 947
- Alard, C., & Lupton, R. H. 1998, *ApJ*, 503, 325
- Aoki, K., Ohtani, H., Yoshida, M., & Kosugi G. 1994, *PASJ*, 46, 539
- Aoki, K., Ohtani, H., Yoshida, M., & Kosugi G. 1996, *AJ*, 111, 140

- Armus, L., Heckman, T. M., & Miley, G. K. 1989, *ApJ*, 347, 727  
 Arribas, S., Mediavilla, E., & Garcia-Lorenzo, B. 1996, *ApJ*, 463, 509  
 Ayani, K., & Iye, M. 1989, *AJ*, 97, 686  
 Binette, L. B., Dopita, M. A., & Tuohy, I. R. 1985, *ApJ*, 297, 476  
 Binggeli, B., Tammann, G. A., & Sandage, A. 1987, *AJ*, 94, 251  
 Bland, J., & Tully, B. 1988, *Nature*, 334, 43  
 Cayatte, V., Kotanyi, C., Balkowski, C., & van Gorkom, J. H. 1994, *AJ*, 107, 1003  
 Chevalier, R., & Clegg, A. 1985, *Nature*, 317, 44  
 Coleman, C. D., Wu, C. -C., & Weedman, D. W. 1980, *ApJS*, 43, 393  
 Colina, L. 1992, *ApJ*, 386, 59  
 Corbin, M., Baldwin, J. A., & Wilson, A. S. 1988, *ApJ*, 334, 584  
 Devine, D., & Bally, J. 1999, *ApJ*, 510, 197  
 Dopita, M. A., & Sutherland, R. A. 1995, *ApJ*, 455, 468  
 Falcke, H., Wilson, A. S., & Simpson, C. 1998, *ApJ*, 502, 199  
 Heckman, T. M., Armus, L., & Miley G. K. 1990, *ApJS*, 74, 833  
 Hernquist, L., & Mihos, J. C. 1995, *ApJ*, 448, 41  
 Hibbard, J. E., Guhathankurta, P., van Gorkom, J. H., & Schweizer, F. 1994, *AJ*, 107, 67  
 Hibbard, J. E., & Yun, M. S. 1999, *AJ*, 118, 162  
 Hummel, E., & Saikia, D. J. 1991, *A&A*, 249, 43  
 Irwin, J. A., Saikia, D. J., & English, J. 2000, *AJ*, 119, 1592  
 Iye, M., et al. 1997, *SPIE*, 2871, 1054  
 Kaifu, N., et al. 2000, *PASJ*, 52, 1  
 Lehnert, M. D., Heckman, T. M., & Weaver, K. A. 1999, *ApJ*, 523, 575  
 McCall, M. L., Rybski, P. M., & Shields, G. A. 1985, *ApJS*, 57, 1  
 Mediavilla, E., & Arribas, S. 1995, *MNRAS*, 276, 579  
 Mihos, J. C. et al. 1995, *ApJ*, 447, L87  
 Miyazaki, S. et al. 1998, *SPIE*, 3355, 363  
 Mizumoto, Y. et al. 2000, *SPIE*, 4009, 429  
 Mulchaey, J. S., Wilson, A. S., & Tsvetanov, Z. 1996, *ApJ*, 467, 197  
 Osterbrock, D. E., 1989, *Astrophysics of Gaseous Nebulae and Active Galactic Nuclei* (University Science Books)  
 Ohyama, Y. et al. 2001, *AJ*, submitted.  
 Padovani, P., & Rafanelli, P. 1988, *A&A*, 205, 53  
 Petitjean, P., & Durret, F. 1993, *A&A*, 277, 365  
 Phillips, M., & Malin, D. F. 1982, *MNRAS*, 199, 905  
 Pogge, R. W. 1988, *ApJ*, 332, 702  
 Pogge, R. W. 1989, *ApJ*, 345, 730  
 Robinson, A. et al. 1994, *A&A*, 291, 351  
 Shopbell, P. L., & Bland-Howthorn, J. 1998, *ApJ*, 493, 129  
 Schull, J. M., & McKee, C. F. 1979, *ApJ*, 227, 131  
 Smith, B. J. 1994, *AJ*, 107, 1695  
 Strickland, D. K., & Stevens, I. R. 2000, *MNRAS*, 314, 511  
 Taniguchi, Y. 1999, *ApJ*, 524, 65  
 Tomisaka, K., & Ikeuchi, S. 1988, *ApJ*, 330, 695  
 Veilleux, S. et al. 1998, in *The central regions of Galaxy and galaxies*, ed. Y. Sofue (Dordrecht: Kluwer), p417  
 Veilleux, S., Bland-Hawthorn, J., Cecil, G., Tully, B., & Miller, S. T. 1999a, *ApJ*, 520, 111(VBCTM)  
 Veilleux, S., Bland-Hawthorn, J., & Cecil, G., 1999b, *AJ*, 118, 2108  
 Walker, I. R., Mihos, J. C., & Hernquist, L., 1996, *ApJ*, 460, 121  
 Yasuda, N., Fukugita, M., & Okamura, S. 1997, *ApJS*, 108, 417  
 Yagi, M. et al. 2000, in *Astronomical Data Analysis Software and Systems IX*, ed. Manset, N., Veillet, N., & Crabtree, D. (Astronomical Society of the Pacific), p510  
 Yoshida, M., & Ohtani, H. 1993, *PASJ*, 45, 407

---

This 2-column preprint was prepared with the AAS L<sup>A</sup>T<sub>E</sub>X macros v5.0.

Fig. 1.— (f1a.jpg) Narrow-band and broad-band images of NGC 4388. In each image, the brightest regions are blacked out in order to enhance the contrast of faint features. North is up and east is to the left. The white, star-like features around the nucleus are artifacts caused by severe saturation of the CCD. a) A continuum subtracted  $H\alpha + [N II]$  image. Faint, highly extended emission-line gas (the very extended emission-line region, or VEELR) is clearly seen in the northeastern quadrant of the galaxy halo. b) A continuum subtracted  $[O III] \lambda 5007 \text{ \AA}$  image. Bright filaments in the inner VEELR can clearly be seen in this image, whereas the outer VEELR is very faint and hardly visible. c) An  $R_c$ -band image. Note that the continuum light distribution of NGC 4388 is asymmetric at a faint surface brightness level. A faint “hump” and “tail” are seen at the southwest edge of the disk and at the west edge of the disk, respectively. d) A  $V$ -band image.

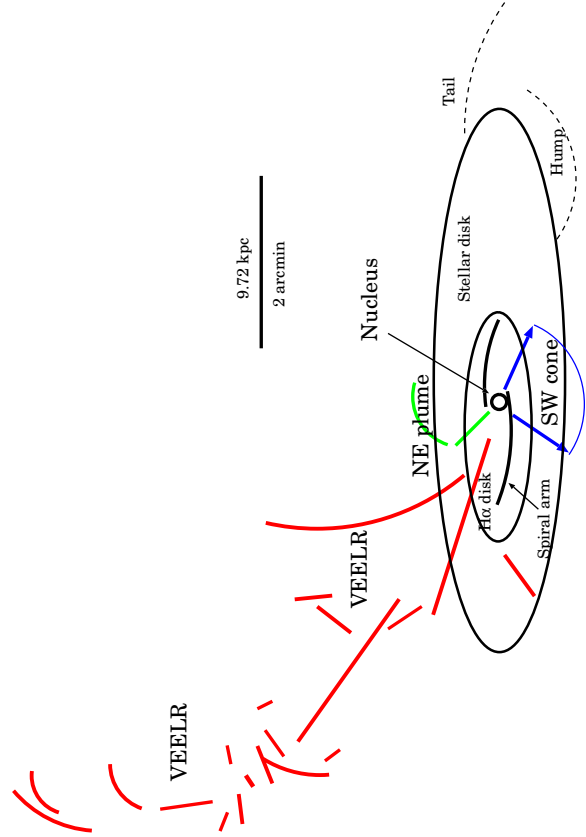


Fig. 2.— A sketch of the distribution of the  $H\alpha$ -emitting gas around NGC 4388.

Fig. 1.— (f1b.jpg)

Fig. 3.— (f3.jpg) Close-up  $H\alpha + [N II]$  images of the VEELR. The detailed structure of the inner VEELR can clearly be seen. The physical parameters of the filaments/clouds numbered in this figure are presented in Table 2.

Fig. 1.— (f1c.jpg)

Fig. 4.— (f4.jpg) A close-up  $[O III]$  image of the NE plume. The FWHM of the PSF of this image  $\approx 0''.8$ , corresponding to 65 pc at the object. Many filaments/clouds are marginally resolved with this spatial resolution.

Fig. 1.— (f1d.jpg)

Fig. 5.— (f5.jpg) A map of the  $I([O III])/I(H\alpha)$  emission-line intensity ratio of NGC 4388. The nuclear ionization cone is clearly revealed in the southwest of the nucleus, and the disk star-forming regions can be seen as low-ionization complexes.

TABLE 1  
JOURNAL OF THE OBSERVATIONS

Filter ID	$\lambda_0(\text{\AA})$	$\Delta\lambda(\text{\AA})$	Date	Exposure Time
N_A_L659	6600	100	2001 April 26	1200 sec $\times$ 8
N_A_L503	5020	100	2001 April 24	1200 sec $\times$ 3
R <sub>c</sub> -band	6700	1000	2001 March 24	240 sec $\times$ 3
V-band	5500	800	2001 March 24	300 sec $\times$ 3

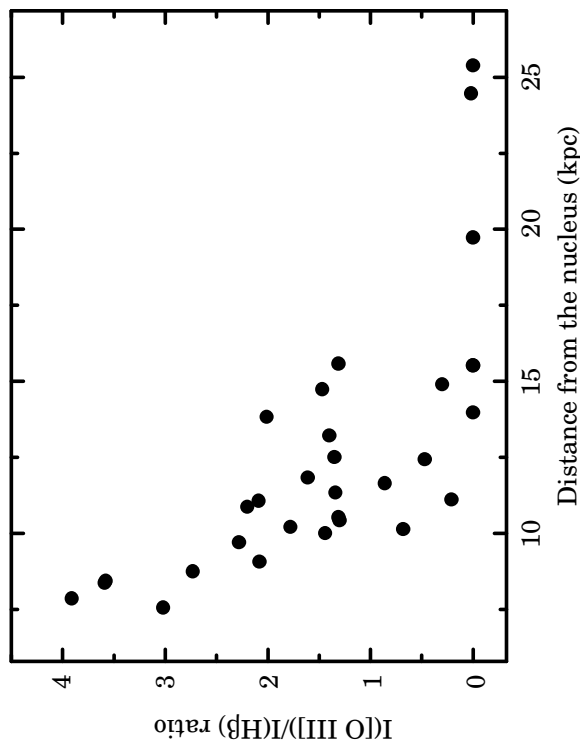


Fig. 6.— The radial dependence of the  $I([\text{O III}])/I(\text{H}\beta)$  ratio of the VEELR.

Fig. 7.— (f7.jpg) An isophote map of the  $R_c$  band image of NGC 4388. The shape of the bulge is boxy rather than spherical. The outer isophotal contour is moderately asymmetrical with respect to the nucleus. A faint hump and tail are seen at the west-southwest edge and at the western edge of the disk, respectively.

TABLE 2  
PHYSICAL PARAMETERS OF THE VEELR GAS CLOUDS

Cloud ID	$f_{\text{H}\alpha+\text{[NII]}}$ <sup>a</sup>	$f_{\text{[OIII]}}$ <sup>b</sup>	$L_{\text{H}\alpha+\text{[NII]}}$ <sup>c</sup>	$L_{\text{[OIII]}}$ <sup>d</sup>	size <sup>e</sup>	distance <sup>f</sup>	$N_e(\text{rms})$ <sup>g</sup>	$M_{\text{gas}} f_V^{-1/2}$ <sup>h</sup>
C1	9.4	8.3	3.1	2.7	160×320	7.6	0.32	3.2
C2	17.7	18.5	5.9	6.2	190×310	8.4	0.37	5.2
C3	22.3	17.8	7.4	5.9	190×360	8.8	0.39	6.2
C4	6.6	4.0	2.2	1.3	110×240	9.1	0.44	1.6
C5	10.7	4.5	3.6	1.5	160×490	10.0	0.28	4.2
C6	3.0	3.4	1.0	1.1	100×240	7.9	0.35	1.0
C7	17.9	18.6	5.9	6.2	5.3 <sup>i</sup>	8.5	0.40	4.8
C8	29.7	19.7	9.9	6.6	190×530	9.7	0.37	8.8
C9	5.2	2.0	1.7	0.7	130×280	10.4	0.32	1.8
C10	6.1	3.2	2.0	1.1	110×240	10.2	0.20	1.6
C11	31.9	19.4	10.6	6.5	210×340	11.1	0.44	7.9
C12	6.5	4.2	2.2	1.4	2.5 <sup>i</sup>	10.9	0.35	2.0
C13	11.2	4.3	3.7	1.4	130×210	10.5	0.54	2.3
C14	12.4	4.9	4.1	1.6	110×400	11.4	0.47	2.9
C15	8.4	4.0	2.8	1.3	130×230	11.9	0.45	2.0
C16	11.9	4.9	4.0	1.6	110×340	13.2	0.50	2.6
C17	20.8	8.2	6.9	2.7	3.6 <sup>i</sup>	12.5	0.53	4.3
C18	15.7	9.2	5.2	3.1	100×630	13.8	0.49	3.5
C19	6.4	2.7	2.1	0.9	100×230	14.8	0.52	1.3
C20	3.2	0.3	1.1	0.1	60×190	14.9	0.60	0.6
C21	4.0	...	1.3	...	100×230	14.0	0.42	1.1
C22	23.4	8.9	7.8	3.0	7.6 <sup>i</sup>	15.6	0.39	6.6
C23	13.1	...	4.4	...	160×890	15.5	0.23	6.3
C24	5.3	...	1.8	...	100×190	15.5	0.51	1.1
C25	9.6	1.3	31.8	4.3	21 <sup>i</sup>	11.8	0.55	22
C26	167.0	33.1	55.6	11.0	32 <sup>i</sup>	10.1	0.5	36
OF-1	87.0	...	28.9	...	117 <sup>i</sup>	18	0.2	49
OF-2	348.0	...	116.0	...	141 <sup>i</sup>	24	0.34	110
OF-3	11.9	...	4.0	...	12.6 <sup>i</sup>	22	0.2	6.1
OF-4	24.3	...	8.1	...	104 <sup>i</sup>	31	0.1	25
OF-5	156.0	...	52.0	...	184 <sup>i</sup>	35	0.2	85

<sup>a</sup>H $\alpha$ + [N II] flux in units of  $10^{-17}$  erg s<sup>-1</sup> cm<sup>-2</sup>.

<sup>b</sup>[O III] $\lambda$ 5007Å flux in units of  $10^{-17}$  erg s<sup>-1</sup> cm<sup>-2</sup>.

<sup>c</sup>H $\alpha$ + [N II] luminosity in units of  $10^{36}$  erg s<sup>-1</sup>. The distance of NGC 4388 is assumed to be 16.7 Mpc.

<sup>d</sup>[O III] $\lambda$ 5007Å luminosity in units of  $10^{36}$  erg s<sup>-1</sup>.

<sup>e</sup>cloud size: pc  $\times$  pc.

<sup>f</sup>distance from the nucleus: kpc.

<sup>g</sup>rms electron density in units of cm<sup>-3</sup>.

<sup>h</sup>ionized gas mass in units of  $10^4 M_{\odot}$ .

<sup>i</sup>cloud volume in units of  $10^6$  pc<sup>3</sup>.

This figure "f1a.jpg" is available in "jpg" format from:

<http://arxiv.org/ps/astro-ph/0110473v1>

This figure "f1b.jpg" is available in "jpg" format from:

<http://arxiv.org/ps/astro-ph/0110473v1>

This figure "f1c.jpg" is available in "jpg" format from:

<http://arxiv.org/ps/astro-ph/0110473v1>

This figure "f1d.jpg" is available in "jpg" format from:

<http://arxiv.org/ps/astro-ph/0110473v1>

This figure "f3.jpg" is available in "jpg" format from:

<http://arxiv.org/ps/astro-ph/0110473v1>

This figure "f4.jpg" is available in "jpg" format from:

<http://arxiv.org/ps/astro-ph/0110473v1>

This figure "f5.jpg" is available in "jpg" format from:

<http://arxiv.org/ps/astro-ph/0110473v1>

This figure "f7.jpg" is available in "jpg" format from:

<http://arxiv.org/ps/astro-ph/0110473v1>